

Automatic learning of hydrogen-bond fixes in an AMBER RNA force field

Thorben Fröhlking,^{†,‡} Vojtěch Mlýnský,^{¶,‡} Michal Janeček,[§] Petra Kührová,^{||}

Miroslav Krepl,^{¶,||} Pavel Banáš,^{||} Jiří Šponer,^{¶,||} and Giovanni Bussi^{*,†}

[†]*Scuola Internazionale Superiore di Studi Avanzati, via Bonomea 265, 34136 Italy*

[‡]*Equal contribution*

[¶]*Institute of Biophysics of the Czech Academy of Sciences, Kralovopolska 135, 612 65
Brno, Czech Republic*

[§]*Department of Physical Chemistry, Faculty of Science, Palacky University, tr. 17
listopadu 12, 771 46, Olomouc, Czech Republic*

^{||}*Regional Centre of Advanced Technologies and Materials, Czech Advanced Technology and
Research Institute (CATRIN), Palacky University Olomouc, Slechtitelu 27, 779 00
Olomouc, Czech Republic*

E-mail: bussi@sissa.it

Abstract

The capability of current force fields to reproduce RNA structural dynamics is limited. Several methods have been developed to take advantage of experimental data in order to enforce agreement with experiments. We herein extend an existing framework, which allows arbitrarily chosen force-field correction terms to be fitted by quantification of the discrepancy between observables back-calculated from simulation and corresponding experiments. We apply a robust regularization protocol to avoid overfitting, and additionally introduce and compare a number of different regularization strategies,

namely L1-, L2-, Kish Size-, Relative Kish Size- and Relative Entropy-penalties. The training set includes a GACC tetramer as well as more challenging systems, namely gc-GAGAgc and gcUUCGgc RNA tetraloops. Specific intramolecular hydrogen bonds in the AMBER RNA force field are corrected with automatically determined parameters that we call gHBfix_{opt} . A validation involving a separate simulation of a system present in the training set (gcUUCGgc) and new systems not seen during training (CAAU and UUUU tetramers) displays improvements regarding native population of the tetraloop as well as good agreement with NMR-experiments for tetramers when using the new parameters. Then we simulate folded RNAs (a kink-turn and L1 stalk rRNA) including hydrogen bond types not sufficiently present in the training set. This allows a final modification of the parameter set which is named gHBfix_{21} and is suggested to be applicable to a wider range of RNA systems.

1 Introduction

As viral pandemics are approached with RNA vaccines¹ and RNA is becoming an increasingly relevant target in therapeutics,² accurate methods for predicting and designing structures and dynamics of nucleic acids are needed to accelerate progress in these fields. Molecular dynamics (MD) simulations in principles allow RNA dynamics to be modeled by computing interactions using empirical force fields and directly solving the equations of motion. However, the capability of MD simulations to predict RNA dynamics is limited both by sampling issues and by force-field accuracy.³ Depending on the size of the system and on the complexity of the investigated conformational transitions, enhanced sampling techniques^{4,5} can help decrease the time-scale issue significantly. However, especially when long simulation time scales or enhanced-sampling methods are employed, the accuracy of the underlying force fields can become a critical issue and can lead to structural ensembles that do not agree with experiment for disordered oligomers^{6,7} or for difficult structural motifs.^{8,9} A number of possible approaches can be used to take advantage of available experimental data in order

to enforce agreement between experiments and simulation data^{10–14} (see also Refs.^{15,16} for recent reviews and Fig. 1 for a schematic). Critical and partly related issues in the application of these methods are (a) avoiding overfitting, which can be moderated by using properly tuned regularization terms,^{13,16} and (b) explicitly modeling experimental errors, which can be naturally done in Bayesian formulations.¹⁴ Both approaches require the degree of confidence one has in experiments and simulations to be tuned. These approaches are expected to generate transferable force fields, and should not be confused with non-transferable ensemble refinements that aim at minimal ensemble corrections without requiring transferability of the resulting force-field form (see, e.g., Refs.^{17–21}). In particular, approaches for transferable force-field refinement are dependent on the functional form of the correction terms to be fixed a priori using chemical intuition. For atomistic MD simulations, these corrections could for instance act on dihedral angle potentials.^{11,13} This is a natural choice, since dihedral angles are usually fitted as a last step, are expected to compensate for all the errors accumulated in other force-field terms, and are naturally connected to the population of different rotamers.²² However, recent works suggested that an imbalance in the relative strength of solute-solute hydrogen bonds might be a key problem of current RNA force fields so that fixing these terms might be more effective than acting on dihedral angles.^{9,23,24} In these works, a limited number of hydrogen bond types were corrected using a so-called generalized hydrogen-bond fix (gHBfix, see Fig. 2), with promising results. This approach allows for minimal corrections that are less likely to present side effects when compared to more extensive reparametrizations of non-bonded interactions²⁵ as shown in Ref.²³. Correction factors for the gHBfix force field, leading to either supporting or disfavoring specific hydrogen bond types, were chosen by trial and error, using a protocol that might be difficult to generalize.²³

In this paper we expand on this idea and show that it is possible to train in an automatic fashion the correction factors associated to hydrogen-bond stabilization in the gHBfix model so as to stabilize the native structure of the difficult⁹ UUCG tetraloop structural motif. To avoid overfitting on the UUCG tetraloop, a tetraloop representative of a different class and

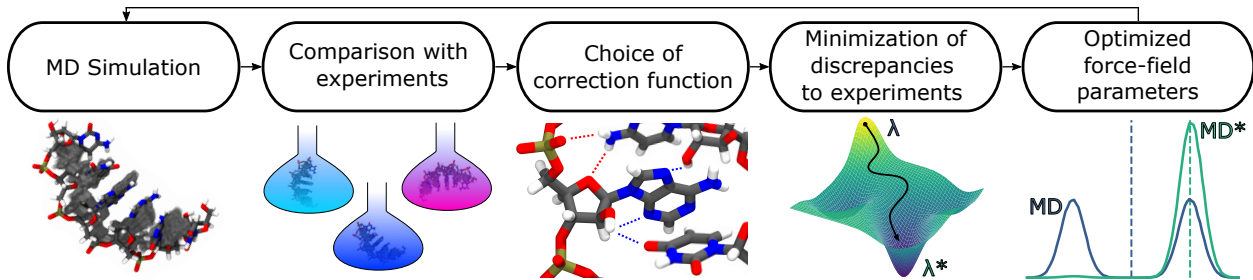


Figure 1: Schematic visualization of the workflow for automatic force-field refinement.¹⁶ After performing MD simulations on training systems for which experimental data are available, experimental quantities are back-calculated and compared with actual experimental data points. One then chooses a basis set for the correction function. The gHBfix corrections²³ are a natural choice to compensate for the possibly incorrect relative stability of hydrogen bonds in the AMBER force field. A numerical minimization is then performed so as to maximize the agreement between simulation and experiment, based on reweighting the simulated trajectories. Ideally, the resulting force field parameters enable new simulations to generate structural ensembles in better agreement with experiment also for systems not included in the training set. If necessary, a new minimization can be performed using a combination of the original and new trajectories, in an iterative fashion.

a flexible tetramer are included in the training set. We use an approach heavily based on that reported in Ref.¹³. As an important extension, here we introduce and compare (a) different forms of the regularization term and (b) different protocols that can be used to perform cross-validation. Training of the 12 parameters of the gHBfix force field is done and demonstrates that this approach can lead to transferable and interpretable force field corrections that match experimental data on a range of systems. A critical assessment of the side effects of the optimized corrections is made. Further tests on carefully chosen folded RNAs allow us to design a final set of parameters (gHBfix21) that is transferable on a wide range of RNA structural motifs. This is an upgrade of the set suggested earlier,²³ which is also known as gHBfix19.⁹ Similarly to the preceding gHBfix19 variant, gHBfix21 should be coupled with the OL3 force field^{26–29} with modified phosphate parameters^{30,31} and OPC water model³² as used here.

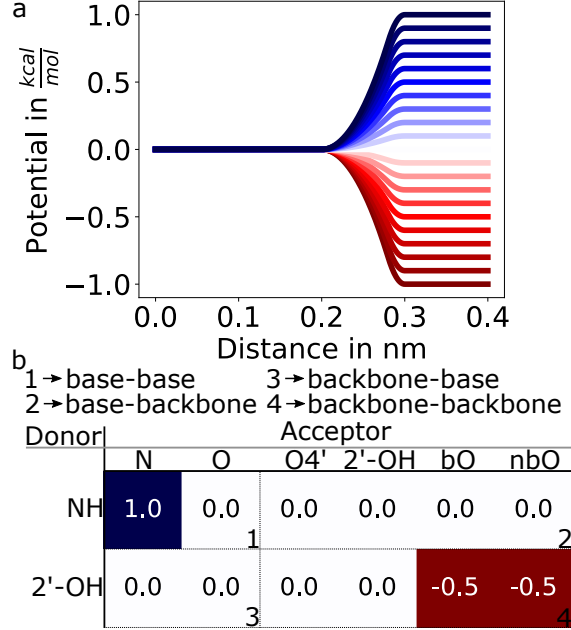


Figure 2: (Panel a) Functional form for the gHBfix-correction potential,²³ displayed as a function of the distance between a hydrogen and the corresponding acceptor. The color scale indicates corrections that could either support (blue) or disfavor (red) a hydrogen bond type. (Panel b) In the present work six possible acceptors and two possible donors are systematically considered, leading to a total of twelve trainable parameters. The numbers show the initial set of parameters (η parameters proposed in Ref.,²³ also referred to as gHBfix19 parameters), here expressed as $k_B T \cdot \lambda$ in kcal/mol. 6 possible acceptors and 2 possible donors are considered in this work, thus leading to a total of 12 trainable parameters. Parameters are colored in blue or red according to the same scale used in panel a.

2 Methods

2.1 Simulation protocols

We performed simulations of several RNA systems, namely (i) GACC, CAAU, and UUUU tetranucleotides, (ii) gcGAGAgc and gcUUCGgc 8-mer tetraloops, (iii) ggcacUUCGgugcc 14-mer tetraloop (PDB ID 2KOC³³), (iv) gcaccguugg (PDB ID 1QC0³⁴) and uuauauauauauaa (PDB ID 1RNA³⁵) RNA duplexes, (v) Kink-turn (Kt-7, PDB ID 1S72,³⁶ 19 nucleotides) and L1 stalk rRNA (PDB ID 3U4M,³⁷ 80 nucleotides) motifs. Starting structures of tetranucleotides and 8-mer tetraloops (in unfolded states) were prepared using Nucleic Acid Builder of AmberTools14³⁸ as one strand of an A-form duplex. The topology and coordinates of simulated systems were prepared using the tLEaP module of AMBER16 program package.³⁹ Several trajectories for analysis were taken from our previous works (see SI Table 1 for full list of systems and simulations). All systems were solvated using a rectangular box of OPC³² water molecules with a minimum distance between box walls and solute of 12 Å. We used the standard OL3 RNA ff²⁶⁻²⁹ with the vdW modification of phosphate oxygens developed in Ref.³⁰ where the affected dihedrals were adjusted as described elsewhere.³¹ AMBER library file of this ff version can be found in Supporting Information of Ref.⁴⁰. Standard MD simulations were run at ≈ 0.15 M KCl using the Joung-Cheatham ion parameters⁴¹ (K^+ : $r = 1.705$ Å, $\epsilon = 0.1937$ kcal/mol, Cl^- : $r = 2.513$ Å, $\epsilon = 0.0356$ kcal/mol). Enhanced sampling simulations of tetranucleotides and tetraloops were run at ≈ 0.15 M and ≈ 1.0 M KCl salt excess, respectively. We used the hydrogen mass repartitioning scheme⁴² allowing a 4-fs integration time step (see Supporting Information of ref.²³ for other details about the simulation protocol). Hydrogen bonds were tuned by various versions of the gHBfix potential²³ (Table 2 in the reference and SI Table 1 of this study). Standard MD simulations were run in AMBER18⁴³ whereas both AMBER18 and GROMACS2018⁴⁴ were used for enhanced sampling simulations. PARMED⁴⁵ was used to convert AMBER topologies and coordinates into GROMACS inputs. Two different enhanced sampling schemes were employed, i.e., standard replica ex-

change solute tempering (REST2)⁴⁶ protocol and well-tempered Metadynamics^{47–49} (MetaD) in combination with REST2 method (ST-MetaD).^{50,51} REST2 simulations were performed at 298 K (the reference replica) with 8 and 16 replicas for tetranucleotides and UUCG 8-mer tetraloop, respectively. Details about settings can be found elsewhere.²³ The scaling factor (λ) values ranged from 1 to 0.601700871 and from 1.0454 to 0.59984 for 8 and 16 replicas, respectively. Those values were chosen to maintain an exchange rate above 20%. The effective solute temperature ranged either from 298 K (8 replicas) or 285 K (16 replicas) to 500 K. REST2 simulations were performed with AMBER GPU MD simulation engine (pmemd.cuda).⁵² ST-MetaD simulations of both GAGA and UUCG 8-mer tetraloops were performed with 12 replicas starting from unfolded single strands and were simulated in the effective temperature range of 298–497 K for 5 μ s per replica. The average acceptance rate was 30% for both tetraloops. The eRMSD metric⁵³ was used as a biased collective variable.⁸ We used eRMSD with an augmented cutoff (set at 3.2) for biasing, which was shown to allow forces to drive the system towards and away from the native state even when nucleobases are far from each other.⁸ In a separate manuscript, we show that using ST-MetaD with MetaD on eRMSD greatly improved the performance of pure ST for RNA tetraloops.⁵¹ Similar conclusions were drawn in Ref.,⁵⁴ where parallel tempering-MetaD^{55,56} with MetaD on the number of native contacts,⁵⁷ a variable highly correlated with eRMSD, was suggested to be significantly more efficient than pure parallel tempering for a GNRA tetraloop. ST-MetaD simulations were carried out using GPU-capable version of GROMACS2018⁴⁴ in combination with PLUMED 2.5^{58,59} (see Section 2.7 for more details about implementation of the gHBfix function within PLUMED code and Table SI 1 in Supporting Information for full list of standard as well as enhanced sampling simulations). In theory, all replicas could be combined using a suitable reweighting procedure. However, to keep the datasets smaller, we here decided to only analyze the reference replica of each replica-exchange simulation. Simulations for the same system performed with different force fields were combined with binless weighted-histogram analysis^{60–62} so as to maximize the statistical efficiency of the

reweighting procedure.

2.2 Experiment-based force-field fitting

We briefly review the formalism behind experiment-based force-field fitting. We here used the procedure discussed in Ref.¹³ Considering $P_0(x)$ as the equilibrium probability distribution of observing a conformation x with the original force field, the refined force field will include a correction in the form $f(x, \{\lambda\})$, where $\{\lambda\}$ is a set of N parameters, leading to an equilibrium distribution $P(x, \{\lambda\}) \propto P_0(x)e^{-f(x, \{\lambda\})}$. We here assume that the correction $f(x, \{\lambda\})$ is a linear combination of N correction functions: $f(x, \{\lambda\}) = \sum_{j=1}^N \lambda_j f_j(x)$. The modified distribution is then used to estimate the expectation value of M experimental observables, defined through forward models $O_i(x)$ that connect the atomic coordinates of conformation x with the experiment. Forward models might correspond for instance to Karplus equations⁶³ or to indicator functions equal to 1 if x is a folded conformation and to 0 otherwise. Their expectation values are computed as $\langle O_i \rangle(\{\lambda\}) = \sum_x O_i(x)P(x, \{\lambda\})$. The cost function, to be minimized in the fitting procedure, can be written as an average of squared discrepancies between these expectation values and the corresponding experimental observations:

$$\chi^2(\{\lambda\}) = \frac{1}{M} \sum_{i=1}^M \left(\frac{\langle O_i \rangle(\{\lambda\}) - O_i^{exp}}{\sigma_i} \right)^2 \quad (1)$$

Here σ_i is an estimate of the experimental error associated to the i -th datapoint.

In this work, the functions f are defined following the gHBfix potential function as formulated in ref.²³ In our implementation, the parameters $\{\lambda\}$ are unitless. However, when reporting them in figures and tables, we convert them to kcal/mol units for clarity, by multiplying them by $k_B T$ where k_B is the Boltzmann constant and T is the simulation temperature. Each of the fitted parameters thus report on how much a given hydrogen bond type is supported (positive) or disfavored (negative).

2.3 Back-calculation of experimental observables

For the two tetraloops, we identified the frames corresponding to native structures using the same procedure used in Ref.,²³ namely considering frames with eRMSD⁵³ from native smaller than 0.7⁶⁴ and all native hydrogen bonds (Watson-Crick hydrogen bonds in the stem and signature hydrogen bonds in the loop, see Figure 1 in Ref.²³). Calling p_i the population of the native state for system i , a contribution to the cost function is computed as:

$$\chi_i^2(\{\lambda\}) = \left(\log \min \left(\frac{p_i(\{\lambda\})}{0.5}, 1 \right) \right)^2. \quad (2)$$

In this manner, a penalty is added whenever the native population is lower than 50%.

For the tetramers we computed the agreement with previously published NMR data^{65–67} using the same procedure as in Ref.²³

2.4 Fitting on multiple systems

The procedure above can be straightforwardly generalized to multiple systems. In practice, separate error functions are computed for each system and their linear combination is taken. Explicitly, if $\chi_i^2(\{\lambda\})$ is the error function for the i -th system, computed using Eq. 1, the total cost function over S systems can be defined as

$$\chi^2(\{\lambda\}) = \sum_{i=1}^S \omega_i \chi_i^2(\{\lambda\}) \quad (3)$$

The prefactor associated to each system in this linear combination (ω_i) allows the weight of each system in the fitting procedure to be tuned. Each of the 3 systems considered in this study is assigned the same weight $\omega_i = 1$, so that they equally contribute to the overall error. Note that these parameters have to be chosen arbitrarily and might have significant impact on the combined χ^2 .

2.5 Regularization terms

The cost function in Eq. 3 can be augmented with a regularization term so as to decrease the degree of overfitting:

$$\tilde{\chi}^2(\{\lambda\}) = \chi^2(\{\lambda\}) + \alpha R(\{\lambda\}) \quad (4)$$

Here R is a function that takes into account how much the force field has been fitted and thus typically grows as the refined force field departs from the reference one. α is a regularization hyperparameter that can be tuned using a cross-validation procedure. We here compare a number of different functional forms for the regularization function $R(\{\lambda\})$. The most common type of regularization is L2 regularization, where the function R is defined as

$$R(\{\lambda\}) = L_2(\{\lambda\}) = \sum_{i=1}^N (\lambda_i - \lambda_i^0)^2 \quad (5)$$

where $\{\lambda^0\}$ are the parameters suggested in the original work,²³ shown in Fig. 2. This type of regularization corresponds to setting a Gaussian prior on the parameters $\{\lambda\}$. Indeed, the logarithm of a Gaussian function of the $\{\lambda\}$'s is proportional to a quadratic function of the $\{\lambda\}$'s. Similarly, a Laplace prior would result in a L1 regularization:

$$R(\{\lambda\}) = L_1(\{\lambda\}) = \sum_{i=1}^N |\lambda_i - \lambda_i^0| \quad (6)$$

L1 regularization leads to more sparse corrections than the L2 regularization, meaning it also offers the potential to identify the most important parameters. In addition to comparing L1 and L2 regularization functions, we also tested a function that depends on the statistical significance of the generated ensemble, namely the inverse of the Kish sample size of the reweighted trajectory:^{68,69}

$$R(\{\lambda\}) = \frac{1}{K(\{\lambda\})} = \sum_t w_t^2 \quad (7)$$

Here w_t depends on $\{\lambda\}$ and represent the reweighting factor for the t -th frame, namely $w_t = \frac{w_{t0}e^{-f(x(t),\{\lambda\})}}{\sum_{t'} w_{t'0}e^{-f(x(t'),\{\lambda\})}}$, where w_{t0} is the weight associated to the original force field, included here to take into account that simulations might have included a bias potential. We notice that a term depending on the Kish size, though different from this one, was also employed in a recent work.¹⁴

We then considered regularization terms that take into account the discrepancy between the prior distribution $P_0(x)$ and the posterior one $P(x)$. We tested the inverse of the relative Kish size, defined as

$$R(\{\lambda\}) = \frac{1}{K_{rel}(\{\lambda\})} = \frac{1}{N_f} \sum_t \frac{w_t^2}{w_{t0}} \quad (8)$$

We also considered the exponential of the negative relative entropy, defined as

$$R(\{\lambda\}) = e^{-S_{rel}(\{\lambda\})} = e^{\sum_t w_t \log \frac{w_t}{w_{t0}}} \quad (9)$$

Although these last two forms are different, they are both expected to grow as the distribution associated to the original force field and that associated to the refined force field depart from each other.

Since the last three regularization terms depend on the analyzed trajectories, they should be combined so as to take into account of how each system is affected by the corrections. We decided to combine them with a LogSumExp (LSE) function,

$$LSE(\{\lambda\}) = \log \sum_{i=1}^S e^{R_i(\{\lambda\})} \quad (10)$$

that effectively picks the largest regularization across all systems. This makes sure that all systems have a sufficient Kish size or a sufficient similarity with the initial ensembles.

The five regularization terms discussed above were modulated by a hyperparameter α . Although in principle they could be combined, we only tested one regularization type at a time. In addition, we added boundaries for the parameter minimizations relative to the

reference parameters (Fig. 2). These boundaries can be interpreted as a L-infinite regularization term ($R = \sum_{i=1}^N \left(\frac{\lambda_i - \lambda_l^0}{\lambda_{max}} \right)^\infty$ with $k_B T \lambda_{max} = 1\text{kcal/mol}$) used on top of one of the five regularization strategies discussed above. In practice, these boundaries avoid divergence in parameters that could become arbitrarily positive or negative.

2.6 Cross-validation strategies

The hyperparameter that tunes the regularization terms discussed in the previous section is chosen so as to maximize the performance in cross-validation. In particular, force field corrections are fitted on a fraction of the available dataset and tested on the left out part of the dataset. We performed three types of cross-validation:

1. Cross-validation on trajectory segments. We split each trajectory in 5 segments. The number of segments is here chosen arbitrarily, and only the ground replica is used, that might contain spurious correlations due to replica exchanges. In principle, one might apply the splitting on continuous (demuxed) trajectories to minimize correlations, and optimize the number of blocks as it is usually done in block analysis.⁷⁰ Then, we minimize the cost function using trajectories where one of the segments was removed, and finally validate the parameters by recomputing the cost function using only the left out segments.
2. Cross-validation on observables. We split the dataset into the 7 observables (GACC: NOEs, uNOEs and scalar-couplings grouped according to the backbone angles γ (backbone1), β or ϵ (backbone2) and sugar torsional angles (sugar), GAGA and UUCG: native population) then minimize the cost function in which the contribution of one observable is ignored and afterwards validate against this left out observable.
3. Cross-validation on systems. We minimize the cost function only including two of the three training systems and then validate the parameters by recomputing the cost function using only the left out system.

In all cases, the cross-validation is repeated by rotating the left-out portion of the data. The first cross-validation strategy allows to check if the parameters would be transferable to a new trajectory simulated for the same set of systems. The other two strategies instead check the transferability to different types of observables or to different systems.

2.7 Implementation

To allow the gHBfix corrections to be used in generic MD codes that might not support the required functional form, we added an implementation within the PLUMED plugin⁵⁸ that is compatible with a large number of MD packages. Specifically, a collective variable has been added that allows the user to provide two groups of atoms and then automatically compute switching functions ranging from -1 (small distance) to 0 (large distance) with a smooth interpolation in the middle. The decision to set this correction to zero for atoms at large distance was taken to make this function compatible to other switching functions implemented in PLUMED and enabling its optimization via neighbor lists. This definition is identical to the one used in the original gHBfix version⁴⁰ except for an additive constant. Multiplicative prefactors for the switching functions can be chosen based on the atom types. This collective variable can be used to analyze hydrogen bond interactions *a posteriori* or to generate bias potentials to correct a simulation on-the-fly.

We here also updated the code 'gHBfix_GenerateInput.cpp' originally published in Ref.²³ (<https://github.com/bussilab/ghbfix-training>), which is printing desired output with the newly implemented gHBfix function for PLUMED code with both required external files (typesTable.dat, scalingParameters.dat). PLUMED input files used in this code are available on PLUMED-NEST (<https://www.plumed-nest.org>), the public repository of the PLUMED consortium,⁷¹ as plumID:21.051.

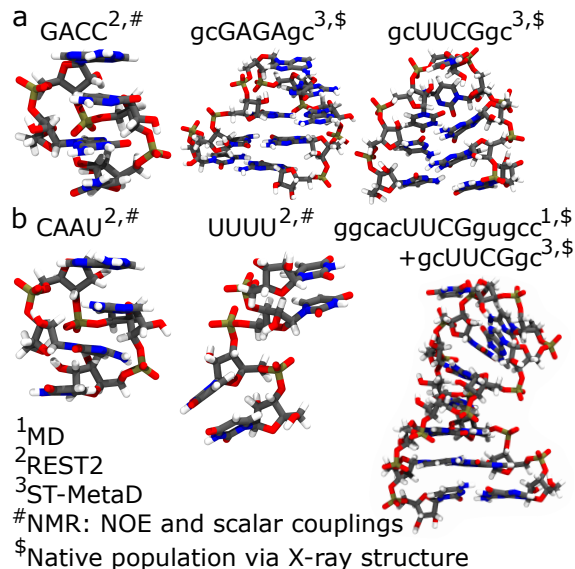


Figure 3: Systems used in training (panel a). For these three systems we performed extensive enhanced sampling simulations. Training was done using NMR data (for GACC) or stability of native structure (for gcGAGAgc and gcUUCGgc). Systems used in validation (panel b). Quantitative validation was done using NMR data (for CAAU and UUUU) or stability of native structure (for gcUUCGgc), whereas qualitative validation was done running long simulations starting from the native structure of a 14-mer with a UUCG loop.³³

3 Results

We here train the 12 gHBfix free parameters corresponding to the 12 types of hydrogen bonds (Fig. 2) by minimizing the discrepancy with respect to the experiment for three systems: two tetraloop motifs with sequence gcUUCGgc and gcGAGAgc and an oligomer with sequence GACC (Fig. 3a). The two tetraloops, or similar ones, were used as folding benchmark in a number of papers (see, *e.g.*, Refs.^{8,9,13,23,25,40,54,72–74}). The GACC tetramer was reported to sample intercalated structures not compatible with experiment,^{7,65} although this artifact can be significantly decreased using modified dihedral potentials^{75,76} or modified water models.^{25,67,74,77} A hyperparameter that controls overfitting is tuned by minimizing the cross-validation error. Several different forms for the regularization term are compared. Once an optimal value for the hyperparameter has been identified, a new fitting is performed including all the training simulations, resulting in a set of optimal parameters that we refer to as gHBfix_{opt}. We then test this set of parameters using additional simulations that include

new systems not used during training and a new simulation of one of the systems used during training (Fig. 3b). Furthermore (see Supporting Information), in order to identify side effects of the $\text{gHBfix}_{\text{opt}}$ parameters, we perform plain MD simulations on carefully chosen folded RNAs (kink-turn and L1 stalk rRNA). These additional simulations allow us to report a new set of parameters (gHBfix21), where one hydrogen bond correction has been manually removed from the $\text{gHBfix}_{\text{opt}}$ parameters, that performs well on a wider range of systems.

3.1 Cross-validation comparison

We first perform a cross-validation test on trajectory segments. In short, we split each trajectory in 5 segments, train the 12 parameters on a subset of 4 segments, and validate against the left-out segment. We repeat the procedure five times, and report the average result. We then repeat the procedure scanning the value of the regularization hyperparameter over 8 orders of magnitude and including 5 different forms for the regularization term. Fig. 4a reports the average error on the training set. By construction, the error increases with the hyperparameter. For four forms of the regularization term, in the limit of large hyperparameters the error of the original force field is recovered. When using the Kish size as a regularization term, instead, this is not guaranteed. Indeed, to maximise the Kish size of the resulting ensemble, thus minimizing the regularization term, one should have uniform weights across all the visited conformations, which is different from using the weights associated to the reference force field. The limit of low hyperparameter corresponds to fitting without any regularization. Fig. 4b reports the average error on the validation set, namely obtained using the trajectory segment that was left-out during the training phase. In this case, the error systematically increases over a wide range of values of the hyperparameter. The minimum error is not appreciably different from the error obtained in absence of regularization. This indicates that, for what concerns the cross-validation on trajectory segments, there is no significant overfitting, and we should expect the obtained parameters to be transferable to a new simulation performed on the same system irrespectively of regularization.

Fig. 4c and d instead report a similar analysis performed by splitting all the input data-points in 7 groups corresponding to the observables, training on a subset of 6 and validating on the left-out observable. In this case, the behavior of the cross-validation error (Fig. 4d) is qualitatively different. In particular, for each of the tested forms of the regularization term, we can clearly identify a specific value of the hyperparameter that minimizes the error on the validation set. For a low value of the hyperparameter instead, we clearly see that the cross-validation error increases. This indicates that, in absence of regularization, one would obtain parameters that would likely be non-transferable to predict new data points. The specific values of the hyperparameter that minimizes the cross-validation error are shown with a star.

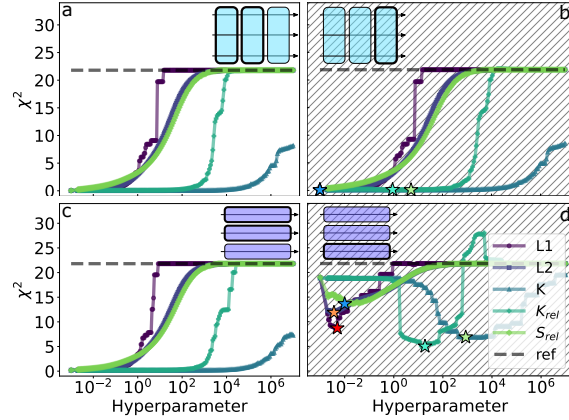


Figure 4: Results of the cross-validation tests on trajectory segments and on observables, using all the tested regularization methods. The error function is evaluated on the training and validation set, using parameters obtained minimizing the error and a scan over a wide range of values for the regularization hyperparameter. Cyan and purple blocks schematize how data are split and used in cross validation. In the first case (panels a and b), the cross-validation is performed keeping out segments of the whole trajectories and using them as a validation set. Error is reported both for the training (panel a) and for the validation (panel b) set. In the second case (panels c and d) the cross-validation is performed keeping out a fraction of the observables and using them as a validation set. Error is reported both for the training (panel c) and for the validation (panel d) set. Error function for the reference force field is reported as a dashed horizontal line.

We notice that, given the different nature of the 5 tested regularization functions, the specific value of the hyperparameter cannot be directly compared. We can however compare the corresponding values of the cross-validation error, that suggests that the maximum trans-

ferability would be obtained using a relative Kish size regularization with a hyperparameter $\alpha = 18.68$. Using this criterion to choose the type of regularization function is legitimate and is equivalent to considering the type of regularization function as an additional categorical hyperparameter that is optimized using the same cross-validation procedure. For further tests we choose the parameters obtained with relative Kish size regularization at this optimal regularization strength, that are also reported in Fig. 5.

| | | | | | | |
|-----------------|----------|---------------------|------|-------|------|------|
| 1→base-base | | 3→backbone-base | | | | |
| 2→base-backbone | | 4→backbone-backbone | | | | |
| Donor | Acceptor | | | | | |
| | N | O | O4' | 2'-OH | bO | nbO |
| NH | 0.3 | 0.8 | -1.0 | -1.0 | -1.0 | 0.1 |
| 2'-OH | 0.8 | 0.9 | -1.0 | -1.0 | -1.5 | -1.5 |

Figure 5: Final set of the 12 trained parameters (*i.e.*, $\text{gHBfix}_{\text{opt}}$) that were obtained fitting on all the systems in the training set using a relative Kish size regularization with a hyperparameter obtained by minimizing the error function of the cross-validation on observables. Parameters are reported as $k_B T \cdot \lambda$ in kcal/mol (corresponding to the η parameters in the gHBfix nomenclature²³) and boxes are colored in blue for attractive terms or in red for repulsive ones.

We also performed a cross-validation on systems, where training is done including two systems and validation on the left-out system (Fig. 6). This analysis allows to clearly identify the contribution of each of the three training systems to the resulting parameters. The left panels show the error on each of the three analyzed systems, highlighting the one that was left-out during training. The gcUUCGgc system has the highest error, as expected.⁹ Interestingly, gcGAGAgc is significantly improved by the presence of gcUUCGgc in the training set. However, the opposite is not true: when gcUUCGgc is excluded from training, the associated validation error displays a minimum that is almost as large as the error in the reference force field. This suggests that the gcUUCGgc native structure is stabilized by types of contact not present in the other systems. We notice that GACC tetramer shows a light overfitting whenever gcUUCGgc is included in the training set. However, the magnitude of this overfitting is moderate, and the final χ^2 error remains below 0.93.

It is also interesting to compare the sets of parameters obtained when regularization is present or absent, and when one of the systems is left out or all the three systems are used (see Fig. 4). When the GACC tetramer is included in the training phase and no regularization is used, some of the parameters become very large and negative. For all considered systems these parameters correspond to hydrogen bonds that are more abundant in the fraction of the ensemble that is less compatible with the experimental observables, and thus should be penalized to improve the result. The particular importance of the concerted effect of these repulsive interactions on the correct representation of GACC can be seen in SI Fig. 1, which shows that removing all repulsive interaction to gHBfix19 parameter significantly increases the χ^2 error of GACC to values > 1 . Importantly, as soon as a regularization term is introduced, the obtained parameters are similar irrespectively of which system has been left out from the training. A fit performed using all the three systems with regularization also reports a similar result (see Fig. 4).

The parameters obtained in all the tested minimizations are similar but not identical in the choice of which interactions should be disfavored and which should be supported. In particular, it emerges that NH-O base-base and 2'-OH N/O sugar-base hydrogen bonds should be supported whenever gcUUCGgc is included in training. The former type corresponds to Watson-Crick hydrogen bonds in the stem and GU wobble pair in loop, whereas the second type corresponds to signature interaction of the UUCG motif.^{9,78} In SI Fig. 2 one can see, that all attractive interactions correspond to contacts that are present in the UUCG native loop. Attractive interactions 2'OH-N/O are exclusively present in the loop region, thus are particularly helpful in correctly stabilizing the challenging UUCG motif. In general, all the hydrogen bonds formed by acceptors located in the sugar or phosphate moieties should be disfavored, with the notable exception of bonds between non-bridging oxygens and NH groups. This might be a consequence of the limited set of systems analyzed in this work, where these moieties are not involved in forming important interactions, as discussed in the next section.

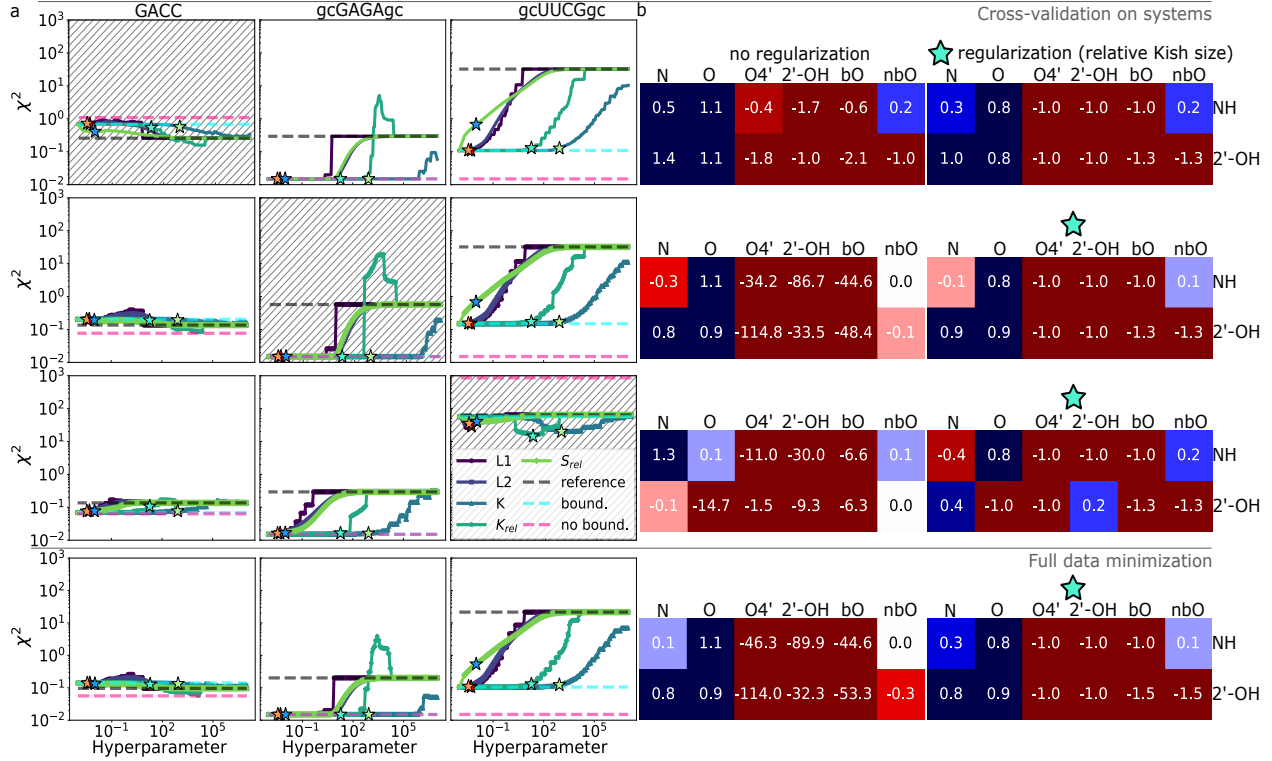


Figure 6: Results of the cross-validation tests on multiple systems, using all the tested regularization methods (left panels). The error function is evaluated on the training (white background) and validation (hatched) set, using parameters obtained minimizing the error and a scan over a wide range of values for the regularization hyperparameter. Error functions for the reference force field (gHBfix19), for an unregularized minimization without boundaries, and for an unregularized minimization with boundaries at ± 1 kcal/mol relative to the original force field are reported as horizontal dashed lines. Parameters associated to each minimization are shown in the right panels, using the same color scale as in Fig. 1, both with and without regularization, as indicated. Parameters obtained with regularization are obtained using the hyperparameter indicated with a star in the cross-validation plots and expressed as $k_B T \cdot \lambda$ in kcal/mol. The last row shows the results for the training error using all available experimental and simulation data during the fitting (left) and the corresponding parameters (right). When regularized (bottom right panel), they correspond to the gHBfix_{opt} parameters derived in this paper.

3.2 Tests using new simulations and additional systems

The parameters obtained in the previous section were thus tested on new simulations. We decided to use the parameters that were obtained fitting on all the training systems using a relative Kish size regularization with a hyperparameter obtained by minimizing the error function of the cross-validation on observables. These parameters are reported in Fig. 5 and are referred to as gHBfix_{opt} . As discussed in the previous section, however, these parameters are largely similar to other sets of parameters obtained in the cross-validation tests.

The first test simulations were performed on three systems (Table 1). In particular, we tested two other tetramers (CAAU and UUUU), for which NMR data are available. CAAU is one of the most challenging tetramers^{23–25,65,67,74,76,79,80} and shows a relatively large χ^2 of 5.37 with gHBfix_{19} ²⁴ as well as 5.0 when reweighting the simulations using gHBfix_{opt} . The test simulation with gHBfix_{opt} reduces the χ^2 value to 3.6, which is an improvement. The UUUU system is relevant since it is known to be highly dynamic in NMR experiments⁶⁵ and was suggested to be too helical in Ref.²⁵ Here the error after reweighting the simulations to gHBfix_{19} is at 1.7, and the simulations with optimized parameters reported here lead to a decreased χ^2 error as well. These results are remarkable in that these two systems were not included in the training set. In addition, we performed new simulations to validate our improvement on the UUCG tetraloop. Specifically, a new ST-MetaD folding simulation of the gcUUCGgc system, using gHBfix_{opt} corrections, but otherwise identical settings as the one used in the training phase, resulted in a native state population of $21 \pm 2\%$. This number is comparable with the native state population of $27 \pm 4\%$ estimated when reweighting the training simulation. Whereas this system was used during training, it is interesting that the parameters were transferable to a direct (non reweighted) simulation, consistently with what we observed in the cross-validation test on trajectory segments (see Fig. 4d). Additionally, we performed a qualitative test on the stability of the UUCG tetraloop by performing 10 independent 20 μs plain MD simulations of a 14-mer initialized in an NMR structure.³³ From SI Fig. 3 it can be seen, that in 9 out of 10 simulations, the native tetraloop structure with all

signature interactions⁹ is stable. We prolonged the single simulation where the native state was partly lost after $\approx 19 \mu s$ and we observed a successful recovery of all contacts at $\approx 20.4 \mu s$. The native state was then maintained until the end of this $30 \mu s$ -long simulation. This is in contrast with the instability observed with other variants of the AMBER force field (see, *e.g.*, Refs.^{9,81}) and with the local conformational dynamics observed with the parameters reported in Ref.²⁵ (see Refs.^{82,83}).

In addition to these systems, we also choose two additional systems for which one specific type of hydrogen bonds that was penalized in our fitted parameters was present in the native structure, namely 2'OH-2'OH bonds. Results are reported in SI Fig. 5 and strongly suggest that the disfavoring of the 2'OH-2'OH contact in gHBfix_{opt} produces undesirable side effects. We thus suggest that the 2'OH-2'OH term should be set to 0.0 kcal/mol (*i.e.*, removed) in simulations of any systems with A-minor, phosphate-in-pocket, and similar interactions with sugar-sugar H-bonding. Our results on the kink-turn and L1 stalk rRNA segments confirm that, after removing this 2'OH-2'OH penalty, no side effects are observed on their native structures. Importantly, the omission of the 2'OH-2'OH correction in gHBfix21 would not visibly compromise the results for the systems that we have used in training or validation (see SI Fig. 4). Remarkably, the test simulations also revealed that the stabilization of the 2'OH-N H-bonds suggested by the fitting done on our training set further stabilizes the native kink-turn structure, with respect to the uncorrected OL3 force field. Namely, the 2'OH-N term eliminates dynamical bifurcation of the most important kink-turn signature interaction between the 2'OH group of the first bulge nucleotide and N1 of the first adenine from the non-canonical stem.⁸⁴

4 Discussion

In this work, we apply a force field fitting strategy that was introduced in a previous work¹³ to the tuning of gHBfix hydrogen bond interaction terms that were introduced in Ref.,²³

Table 1: χ^2 -errors and native populations for the training and testing simulations. For the training simulations, we report both the direct results of the simulations (gHBfix19 column) and the results predicted by reweighting those simulations to the gHBfix_{opt} parameters displayed in Fig. 5) (gHBfix_{opt} column). Notice that for GACC the results are obtained combining simulations performed with multiple parameter sets (see text for details). For the validation simulations, we report both the direct results of the simulations (gHBfix_{opt} column) and the results predicted by reweighting those simulations to the gHBfix parameters with reweighting (gHBfix19 column).

| System (observable) | gHBfix19 | gHBfix _{opt} |
|------------------------------|----------------------------------------|-----------------------------|
| <i>Training simulation</i> | | |
| GACC (χ^2 -NMR) | 0.24 ^{a,b} | 0.33 ^d |
| gcGAGAgc (native population) | $24 \pm 1\%$ ^c | $66 \pm 3\%$ ^d |
| gcUUCGgc (native population) | $0.02 \pm 0.002\%$ ^c | $27 \pm 4\%$ ^d |
| <i>Validation simulation</i> | | |
| gcUUCGgc (native population) | $0.003 \pm 0.004\%$ ^d | $21 \pm 2\%$ ^{c,e} |
| CAAU (χ^2 -NMR) | 5.00 ^d (5.37 ^f) | 3.64 ^{b,e} |
| UUUU (χ^2 -NMR) | 1.73 ^d (1.63 ^f) | 1.48 ^{b,e} |

^a Results are obtained combining simulations ^c ST-metadynamics simulation.

performed with multiple parameter sets (see ^d Reweighted results.
methods for details).

^b REST2 simulation.

^e Simulations with gHBfix_{opt} parameters.

^f Simulations with gHBfix19 parameters.²⁴

obtaining parameters that we call here $\text{gHBfix}_{\text{opt}}$. Specifically, experimental data for two tetraloops and one tetramer are used to fit corrections that are then tested on newer simulations of one of the two tetraloops and on two tetramers not seen during fitting. The obtained parameters result in a significant stabilization of the difficult UUCG tetraloop. Additional tests are performed on systems where 2'OH-2'OH H-bonds are essential for stabilization, since this H-bond is not present in any of the RNA structures considered in the training set, indicating general applicability of the gHBfix_{21} parameter set on a wide range of RNA systems. Using gHBfix_{21} instead of $\text{gHBfix}_{\text{opt}}$ does not compromise the performance for any of the training and validation systems while it eliminates all side-effects on the native structures of kink-turn and L1 stalk rRNA. Scripts that can be used to repeat the fits and reproduce the figures of this article can be found at <https://github.com/bussilab/ghbfix-training>.

When compared with Ref.,¹³ we report a number of methodological improvements. First, we test five different regularization strategies. Two of them (L1 and L2) are standard in the machine learning community and can be directly interpreted as prior distributions on the parameters aimed at keeping them small (L2) or sparse (L1). We also test two additional strategies that are aimed at keeping the resulting reweighted ensemble as close as possible to the original one (relative entropy and relative Kish size). Interestingly, there is an analogy between using the relative entropy as a regularization term and the Bayesian experimental restraints introduced in Ref.¹⁹ Indeed, in both cases, among the multiple possible ensembles that are equally in agreement with experiment, the method will pick the one that is as close as possible to the original ensemble. At variance with Ref.,¹⁹ however, the approach introduced here is aimed at deriving transferable corrections. Finally, we test the possibility to regularize using the inverse of the Kish size, which allows to keep the resulting reweighted ensemble as statistically rich as possible. A similar idea was proposed in Ref.,¹⁴ though using a different functional form. We notice that in some cases the initial trajectories are generated using algorithms that provide conformations associated with a weight. This happens, for instance, when using enhanced sampling methods where a bias is applied or when combining

trajectories obtained with different force fields using binless weighted histograms.^{60–62} In these cases, using a Kish size regularization makes the ensembles as uniform as possible, and thus the result might depend significantly on which ensembles were sampled originally and which enhanced sampling strategy was used. In the last three discussed strategies (relative entropy, relative Kish size, and Kish size), the penalty introduced by the regularization term does not depend only on the parameters but also on the data, and thus can be interpreted as a form of representational regularizations.^{85,86}

Using as fitting coefficients the prefactors associated to the gHBfix corrections,²³ makes their interpretation straightforward, as they directly report on how much each hydrogen bond type is to be supported (positive coefficient) or penalized (negative coefficient). When one of the trained coefficients diverges, the weight of frames where one interaction of that type is either present (for a negative coefficient) or absent (for a positive coefficient) are effectively removed from the ensemble. The result is thus mildly depending on the exact value of the coefficients. This means that, for selected training sets, one or more of the parameters might diverge with some of the regularization strategies mentioned above. This might lead to forces of infinite magnitude if these corrections were applied to a new simulation. To avoid this type of issues, we added a L-infinite-like regularization term that enforce all the parameters to be within preassigned boundaries. Namely, we favor or disfavor any of the corrected pairs by at most 1 kcal/mol. The possibility to automatically repeat the training using different subsets of systems allows one to judge the contribution of each system in the overall fitting. Similarly, it is easy to repeat the training manually removing some of the correction, so as to identify the role of each term.

Another concept that is introduced here is that of performing a cross-validation over trajectory segments. This allows one to assess how much the parameters would be generalizable to a new trajectory for the same systems. This is a useful criterion to decrease the impact of errors due to finite sampling. In our dataset, even in absence of regularization, no significant overfitting on the trajectory segments emerges, indicating that our trajectories

are long enough to be used in this training procedure. However, for more complex systems or for shorter trajectories, this might not be true.

The optimized parameters, that we refer to as gHBfix_{opt} parameters, perform well both in a new simulation of the difficult UUCG tetraloop and in the simulation of two tetramers not seen during training, confirming that parameters are transferable. For the UUCG tetraloop, we remark that the native state population reported here is higher than the one reported in Ref.²⁵ Importantly, the G_{L4} bulge out structure that has been described both for the parameters of Ref.²⁵ (see Refs.^{64,82,83}) and for previous variants of the AMBER force field,^{7,13,73} and that is not compatible with experimental solution data,^{33,83,87} is not populated in our plain MD simulations. The capability of the flexible functional form of the gHBfix correction to directly stabilize the signature interactions present in the native structures with no or minimal side effects, coupled with the explicit inclusion of a UUCG tetraloop in our training set, allows for the required corrections to be automatically detected. We speculate that this result can be only achieved with such a flexible functional form. A folding simulation using the proposed parameters and the full 14-mer system is left as a subject for a future work.

It is additionally important to notice that some interaction types were not present in the native structures of the systems used in our training set. These interactions were thus maximally penalized by the training procedure. Particularly relevant is the case of interactions between a pair of 2'OH groups. Sugar-sugar H-bonding is an important component of A-minor and all other types of ribose zipper interactions.^{3,88-91} Sugar-sugar interactions are omnipresent in folded RNAs and the A-minor interaction is actually the most abundant RNA tertiary interaction used by evolution.^{3,92} These interactions are indeed crucial for maintaining, for example, the native fold for a kink-turn motif and for the L1 stalk rRNA, which in turn includes two kink-turn motifs. In order to simulate systems where these interactions play an important role, the optimized parameters should be manually modified. In theory, one could directly include kink-turns in the training set. However, trajectories where the native structure is folded and unfolded at equilibrium would be required to estimate the

effect of a correction on the stability of the native structure using a reweighting procedure. Whereas this might be possible at least for the kink turn studied here, it would be extremely expensive and will be left as a subject for a future work. We here decided to manually remove a single parameter, and to validate it on the kink-turn motif using standard MD simulations. The resulting gHBfix21 parameter set is proposed to be applicable on a wider range of systems.

We notice that with the present gHBfix_{opt} version the kink-turn and L1 stalk rRNA were significantly destabilized, however not to the same extent as with another recent reparametrization of the RNA force field,²⁵ as shown in Ref.²³ This might be related to the fact that the parameters introduced in Ref.²⁵ were optimized to correctly fold structural motifs similar to the tetraloops used in our training set. This observation corroborates the fact that the training set should be as heterogeneous as possible to avoid overfitting.¹⁶ However, the flexibility of the method allows parameters to be adjusted so as to manually remove some of the terms and train again the remaining ones. With the adjusted gHBfix21 parameter set all side-effects on the kink-turn and L1 stalk rRNA were eliminated.

An important advantage of the gHBfix functional form is its modularity, namely the fact that it is possible to act on specific hydrogen bond types while minimizing the indirect effects on others. In fact, it is separated from all the other force-field terms. In order to allow flexible adjustments to the gHBfix_{opt} parameter based on some detailed system knowledge, in the SI we show fitted force-fields which are omitting specific interactions, or reduce upper and lower bound of the parameters during fitting. Additionally, the SI provides a fitting script, which allows users to specify interactions to remain unchanged or within a certain magnitude and find a new force field matching these requirements (SI 8.5). In case one is concerned about too large changes of the relative stability of AU and GC pairs with the gHBfix_{opt} parameters, in SI Fig. 4 we offer a gHBfix_{opt}-version with a reduced magnitude of the NH-O interaction and we also show its expected effects on the training set. In other words, the users can modify the gHBfix in specific projects in a system-specific manner.

We recall that the present gHBfix21 version was derived to be applied on top of the basic AMBER OL3 RNA force field,^{27–29} with phosphate oxygen corrections^{30,31} and combined with the OPC water model.³²

Future studies should investigate whether non-linear functions can additionally improve force fields by allowing more functional flexibility, *e.g.*, in the form artificial neural networks, when one attempts to find correction potentials for more extensive databases of RNA dynamics.

5 Acknowledgement

This work was supported by Czech Science Foundation (20-16554S to V.M., M.K. and J.S.).

Supporting Information Available

Eight sections discussing (1) all simulations analyzed in this paper, (2) sensitivity analysis on gHBfix_{opt}, (3) favored interaction types of gHBfix_{opt}, (4) standard simulations of the 14-mer ggcacUUCGgugcc system carried out with gHBfix19 and gHBfix_{opt}, (5) custom constraints on corrections in order to take into account possible side-effects, (6) MD simulations of kink-turns Kt-7 and L1 stalk rRNA, (7) helical properties in simulations on RNA duplexes corrected with gHBfix_{opt}, (8) the provided scripts allowing to obtain all published results of this study.

References

- (1) Teijaro, J. R.; Farber, D. L. COVID-19 vaccines: modes of immune activation and future challenges. *Nat. Rev. Immunol.* **2021**, *21*, 195–197.
- (2) Matsui, M.; Corey, D. R. Non-coding RNAs as drug targets. *Nat. Rev. Drug. Discov.* **2017**, *16*, 167–179.

- (3) Šponer, J.; Bussi, G.; Krepl, M.; Banáš, P.; Bottaro, S.; Cunha, R. A.; Gil-Ley, A.; Pinamonti, G.; Poblete, S.; Jurečka, P.; Walter, N. G.; Otyepka, M. RNA structural dynamics as captured by molecular simulations: a comprehensive overview. *Chem. Rev.* **2018**, *118*, 4177–4338.
- (4) Bernardi, R. C.; Melo, M. C.; Schulten, K. Enhanced sampling techniques in molecular dynamics simulations of biological systems. *Biochim. Biophys. Acta, Gen. Subj.* **2015**, *1850*, 872–877.
- (5) Mlýnský, V.; Bussi, G. Exploring RNA structure and dynamics through enhanced sampling simulations. *Curr. Opin. Struc. Biol.* **2018**, *49*, 63–71.
- (6) Condon, D. E.; Kennedy, S. D.; Mort, B. C.; Kierzek, R.; Yildirim, I.; Turner, D. H. Stacking in RNA: NMR of Four Tetramers Benchmark Molecular Dynamics. *J. Chem. Theory Comput.* **2015**, *11*, 2729.
- (7) Bergonzo, C.; Henriksen, N. M.; Roe, D. R.; Cheatham, T. E. Highly sampled tetranucleotide and tetraloop motifs enable evaluation of common RNA force fields. *RNA* **2015**, *21*, 1578–1590.
- (8) Bottaro, S.; Banáš, P.; Šponer, J.; Bussi, G. Free Energy Landscape of GAGA and UUCG RNA Tetraloops. *J. Phys. Chem. Lett.* **2016**, *7*, 4032.
- (9) Mráziková, K.; Mlynsky, V.; Kuhrova, P.; Pokorná, P.; Kruse, H.; Krepl, M.; Otyepka, M.; Banas, P.; Sponer, J. UUCG RNA Tetraloop as a Formidable Force-Field Challenge for MD Simulations. *J. Chem. Theory Comput.* **2020**, *16*, 7601–7617.
- (10) Norgaard, A. B.; Ferkinghoff-Borg, J.; Lindorff-Larsen, K. Experimental parameterization of an energy function for the simulation of unfolded proteins. *Biophys. J.* **2008**, *94*, 182–192.

- (11) Li, D.-W.; Brüschweiler, R. Iterative optimization of molecular mechanics force fields from NMR data of full-length proteins. *J. Chem. Theory Comput.* **2011**, *7*, 1773–1782.
- (12) Cesari, A.; Gil-Ley, A.; Bussi, G. Combining simulations and solution experiments as a paradigm for RNA force field refinement. *J. Chem. Theory Comput.* **2016**, *12*, 6192–6200.
- (13) Cesari, A.; Bottaro, S.; Lindorff-Larsen, K.; Banáš, P.; Šponer, J.; Bussi, G. Fitting corrections to an RNA force field using experimental data. *J. Chem. Theory Comput.* **2019**, *15*, 3425–3431.
- (14) Köfinger, J.; Hummer, G. Empirical optimization of molecular simulation force fields by Bayesian inference. 2021; ChemRxiv, doi:10.33774/chemrxiv-2021-tsbj3-v.
- (15) Orioli, S.; Larsen, A. H.; Bottaro, S.; Lindorff-Larsen, K. How to learn from inconsistencies: Integrating molecular simulations with experimental data. *Prog. Mol. Biol. Transl.* **2020**, *170*, 123–176.
- (16) Fröhlking, T.; Bernetti, M.; Calonaci, N.; Bussi, G. Toward empirical force fields that match experimental observables. *J. Chem. Phys.* **2020**, *152*, 230902.
- (17) Pitera, J. W.; Chodera, J. D. On the use of experimental observations to bias simulated ensembles. *J. Chem. Theory Comput.* **2012**, *8*, 3445–3451.
- (18) White, A. D.; Voth, G. A. Efficient and minimal method to bias molecular simulations with experimental data. *J. Chem. Theory Comput.* **2014**, *10*, 3023–3030.
- (19) Hummer, G.; Köfinger, J. Bayesian ensemble refinement by replica simulations and reweighting. *J. Chem. Phys.* **2015**, *143*, 12B634-1.
- (20) Bonomi, M.; Camilloni, C.; Cavalli, A.; Vendruscolo, M. MetaInference: A Bayesian inference method for heterogeneous systems. *Sci. Adv.* **2016**, *2*, e1501177.

- (21) Cesari, A.; Reißer, S.; Bussi, G. Using the maximum entropy principle to combine simulations and solution experiments. *Computation* **2018**, *6*, 15.
- (22) Richardson, J. S.; Schneider, B.; Murray, L. W.; Kapral, G. J.; Immormino, R. M.; Headd, J. J.; Richardson, D. C.; Ham, D.; HersHKovits, E.; Williams, L. D., et al. RNA backbone: consensus all-angle conformers and modular string nomenclature (an RNA Ontology Consortium contribution). *RNA* **2008**, *14*, 465.
- (23) Kührová, P.; Mlýnský, V.; Zgarbová, M.; Krepl, M.; Bussi, G.; Best, R. B.; Otyepka, M.; Šponer, J.; Banáš, P. Improving the performance of the AMBER RNA force field by tuning the hydrogen-bonding interactions. *J. Chem. Theory Comput.* **2019**, *15*, 3288–3305.
- (24) Mlýnský, V.; Kührová, P.; Kühn, T.; Otyepka, M.; Bussi, G.; Banáš, P.; Šponer, J. Fine-tuning of the AMBER RNA Force Field with a New Term Adjusting Interactions of Terminal Nucleotides. *J. Chem. Theory Comput.* **2020**, *16*, 3936–3946.
- (25) Tan, D.; Piana, S.; Dirks, R. M.; Shaw, D. E. RNA force field with accuracy comparable to state-of-the-art protein force fields. *Proc. Natl. Acad. Sci. U.S.A.* **2018**, *115*, E1346–E1355.
- (26) Cornell, W. D.; Cieplak, P.; Bayly, C. I.; Gould, I. R.; Merz, K. M.; Ferguson, D. M.; Spellmeyer, D. C.; Fox, T.; Caldwell, J. W.; Kollman, P. A. A Second Generation Force Field for the Simulation of Proteins, Nucleic Acids, and Organic Molecules J. Am. Chem. Soc. 1995, *117*, 5179-5197. *J. Am. Chem. Soc.* **1996**, *118*, 2309–2309.
- (27) Wang, J.; Cieplak, P.; Kollman, P. A. How well does a restrained electrostatic potential (RESP) model perform in calculating conformational energies of organic and biological molecules? *J. Comput. Chem.* **2000**, *21*, 1049–1074.
- (28) Pérez, A.; Marchán, I.; Svozil, D.; Šponer, J.; Cheatham, T. E.; Laughton, C. A.;

- Orozco, M. Refinement of the AMBER Force Field for Nucleic Acids: Improving the Description of α/γ Conformers. *Biophys. J.* **2007**, *92*, 3817–3829.
- (29) Zgarbová, M.; Otyepka, M.; Šponer, J.; Mládek, A.; Banáš, P.; Cheatham, T. E.; Jurečka, P. Refinement of the Cornell et al. Nucleic Acids Force Field Based on Reference Quantum Chemical Calculations of Glycosidic Torsion Profiles. *J. Chem. Theory Comput.* **2011**, *7*, 2886–2902.
- (30) Steinbrecher, T.; Latzer, J.; Case, D. A. Revised AMBER Parameters for Bioorganic Phosphates. *J. Chem. Theory Comput.* **2012**, *8*, 4405–4412.
- (31) Mlýnský, V.; Kührová, P.; Zgarbová, M.; Jurečka, P.; Walter, N. G.; Otyepka, M.; Šponer, J.; Banáš, P. Reactive Conformation of the Active Site in the Hairpin Ribozyme Achieved by Molecular Dynamics Simulations with ϵ/ζ Force Field Reparametrizations. *J. Phys. Chem. B* **2015**, *119*, 4220–4229.
- (32) Izadi, S.; Anandakrishnan, R.; Onufriev, A. V. Building Water Models: A Different Approach. *J. Phys. Chem. Lett.* **2014**, *5*, 3863–3871.
- (33) Nozinovic, S.; Fürtig, B.; Jonker, H. R.; Richter, C.; Schwalbe, H. High-resolution NMR structure of an RNA model system: the 14-mer cUUCGg tetraloop hairpin RNA. *Nucleic Acids Res.* **2010**, *38*, 683.
- (34) Klosterman, P. S.; Shah, S. A.; Steitz, T. A. Crystal structures of two plasmid copy control related RNA duplexes: an 18 base pair duplex at 1.20 Å resolution and a 19 base pair duplex at 1.55 Å resolution. *Biochemistry* **1999**, *38*, 14784–14792.
- (35) Dock-Bregeon, A.; Chevrier, B.; Podjarny, A.; Johnson, J.; De Bear, J.; Gough, G.; Gilham, P.; Moras, D. Crystallographic structure of an RNA helix:[U (UA) 6A] 2. *J. Mol. Biol.* **1989**, *209*, 459–474.

- (36) Klein, D.; Moore, P.; Steitz, T. The roles of ribosomal proteins in the structure assembly, and evolution of the large ribosomal subunit. *J. Mol. Biol.* **2004**, *340*, 141–177.
- (37) Tishchenko, S.; Gabdulkhakov, A.; Nevskaya, N.; Sarskikh, A.; Kostareva, O.; Nikonova, E.; Sycheva, A.; Moshkovskii, S.; Garber, M.; Nikonov, S. High-resolution crystal structure of the isolated ribosomal L1 stalk. *Acta Crystallogr. D* **2012**, *68*, 1051–1057.
- (38) Case, D. A.; Cheatham III, T. E.; Darden, T.; Gohlke, H.; Luo, R.; Merz Jr, K. M.; Onufriev, A.; Simmerling, C.; Wang, B.; Woods, R. J. The Amber biomolecular simulation programs. *J. Comput. Chem.* **2005**, *26*, 1668–1688.
- (39) Case, D. A.; Betz, R. M.; Cerutti, D. S.; III, T. E. C.; Darden, T. A.; Duke, R. E.; Giese, T. J.; H. Gohlke, A. W. G.; Homeyer, N.; Izadi, S.; Janowski, P.; Kaus, J.; Kovalenko, A.; Lee, T. S.; LeGrand, S.; Li, P.; Lin, C.; Luchko, T.; Luo, R.; Madej, B.; Mermelstein, D.; Merz, K. M.; Monard, G.; Nguyen, H.; Nguyen, H. T.; Omelyan, I.; Onufriev, A.; Roe, D. R.; Roitberg, A.; Sagui, C.; Simmerling, C. L.; Botello-Smith, W. M.; J. Swails, R. C. W.; Wang, J.; Wolf, R. M.; Wu, X.; Xiao, L.; Kollman, P. A. AMBER 2016, University of California, San Francisco.
- (40) Kührová, P.; Best, R. B.; Bottaro, S.; Bussi, G.; Šponer, J.; Otyepka, M.; Banáš, P. Computer Folding of RNA Tetraloops: Identification of Key Force Field Deficiencies. *J. Chem. Theory Comput.* **2016**, *12*, 4534–4548.
- (41) Joung, I. S.; Cheatham, T. E. Determination of Alkali and Halide Monovalent Ion Parameters for Use in Explicitly Solvated Biomolecular Simulations. *J. Phys. Chem. B* **2008**, *112*, 9020–9041.
- (42) Hopkins, C. W.; Le Grand, S.; Walker, R. C.; Roitberg, A. E. Long-Time-Step Molecular Dynamics through Hydrogen Mass Repartitioning. *J. Chem. Theory Comput.* **2015**, *11*, 1864–1874.

- (43) Case, D. A.; Ben-Shalom, I. Y.; Brozell, S. R.; Cerutti, D. S.; III, T. E. C.; Cruzeiro, V. W. D.; T. A. Darden, R. E. D.; Ghoreishi, D.; Gilson, M. K.; Gohlke, H.; Goetz, A. W.; Greene, D.; Harris, R.; Homeyer, N.; Y. Huang, S. I.; Kovalenko, A.; Kurtzman, T.; Lee, T. S.; LeGrand, S.; Li, P.; Lin, C.; Liu, J.; Luchko, T.; Luo, R.; Mermelstein, D. J.; Merz, K. M.; Miao, Y.; Monard, G.; Nguyen, C.; Nguyen, H.; Omelyan, I.; Onufriev, A.; Pan, F.; Qi, R.; Roe, D. R.; Roitberg, A.; Sagui, C.; Schott-Verdugo, S.; Shen, J.; Simmerling, C. L.; Smith, J.; SalomonFerrer, R.; Swails, J.; Walker, R. C.; Wang, J.; Wei, H.; Wolf, R. M.; Wu, X.; Xiao, L.; York, D. M.; Kollman, P. A. AMBER 2018, University of California, San Francisco.
- (44) Abraham, M. J.; Murtola, T.; Schulz, R.; Páll, S.; Smith, J. C.; Hess, B.; Lindahl, E. GROMACS: High performance molecular simulations through multi-level parallelism from laptops to supercomputers. *SoftwareX* **2015**, *1*, 19–25.
- (45) Shirts, M. R.; Klein, C.; Swails, J. M.; Yin, J.; Gilson, M. K.; Mobley, D. L.; Case, D. A.; Zhong, E. D. Lessons learned from comparing molecular dynamics engines on the SAMPL5 dataset. *J. Comput. Aided Mol. Des.* **2017**, *31*, 147–161.
- (46) Wang, L.; Friesner, R. A.; Berne, B. J. Replica Exchange with Solute Scaling: A More Efficient Version of Replica Exchange with Solute Tempering (REST2). *J. Phys. Chem. B* **2011**, *115*, 9431–9438.
- (47) Laio, A.; Parrinello, M. Escaping free-energy minima. *Proc. Natl. Acad. Sci. U.S.A.* **2002**, *99*, 12562–12566.
- (48) Barducci, A.; Bussi, G.; Parrinello, M. Well-tempered metadynamics: a smoothly converging and tunable free-energy method. *Phys. Rev. Lett.* **2008**, *100*, 020603.
- (49) Bussi, G.; Laio, A. Using metadynamics to explore complex free-energy landscapes. *Nat. Rev. Phys.* **2020**, *2*, 200–212.

- (50) Camilloni, C.; Provasi, D.; Tiana, G.; Broglia, R. A. Exploring the protein G helix free-energy surface by solute tempering metadynamics. *Proteins* **2008**, *71*, 1647–1654.
- (51) Mlynsky, V.; Janecek, M.; Kuhrova, P.; Frohlik, T.; Otyepka, M.; Bussi, G.; Banas, P.; Sponer, J. Towards Convergence in Folding Simulations of RNA Tetraloops: Comparison of Enhanced Sampling Techniques and Effects of Force Field Corrections. *bioRxiv preprint*, doi:10.1101/2021.11.30.470631 **2021**,
- (52) Mermelstein, D. J.; Lin, C.; Nelson, G.; Kretsch, R.; McCammon, J. A.; Walker, R. C. Fast and flexible gpu accelerated binding free energy calculations within the amber molecular dynamics package. *J. Comput. Chem.* **2018**, *39*, 1354–1358.
- (53) Bottaro, S.; Di Palma, F.; Bussi, G. The role of nucleobase interactions in RNA structure and dynamics. *Nucleic Acids Res.* **2014**, *42*, 13306.
- (54) Zerze, G. H.; Piaggi, P. M.; Debenedetti, P. G. A Computational Study of RNA Tetraloop Thermodynamics, Including Misfolded States. *J. Phys. Chem. B* ASAP, <https://doi.org/10.1021/acs.jpcb.1c08038>.
- (55) Bonomi, M.; Parrinello, M. Enhanced sampling in the well-tempered ensemble. *Phys. Rev. Lett.* **2010**, *104*, 190601.
- (56) Bussi, G.; Gervasio, F. L.; Laio, A.; Parrinello, M. Free-energy landscape for β hairpin folding from combined parallel tempering and metadynamics. *J. Am. Chem. Soc.* **2006**, *128*, 13435–13441.
- (57) Best, R. B.; Hummer, G.; Eaton, W. A. Native contacts determine protein folding mechanisms in atomistic simulations. *Proc. Natl. Acad. Sci. U.S.A.* **2013**, *110*, 17874–17879.
- (58) Tribello, G. A.; Bonomi, M.; Branduardi, D.; Camilloni, C.; Bussi, G. PLUMED 2: New feathers for an old bird. *Comput. Phys. Commun.* **2014**, *185*, 604–613.

- (59) Bussi, G. Hamiltonian replica exchange in GROMACS: a flexible implementation. *Mol. Phys.* **2014**, *112*, 379–384.
- (60) Souaille, M.; Roux, B. Extension to the weighted histogram analysis method: combining umbrella sampling with free energy calculations. *Comput. Phys. Commun.* **2001**, *135*, 40–57.
- (61) Shirts, M. R.; Chodera, J. D. Statistically optimal analysis of samples from multiple equilibrium states. *J. Chem. Phys.* **2008**, *129*, 124105.
- (62) Tan, Z.; Gallicchio, E.; Lapelosa, M.; Levy, R. M. Theory of binless multi-state free energy estimation with applications to protein-ligand binding. *J. Chem. Phys.* **2012**, *136*, 144102.
- (63) Karplus, M. Vicinal proton coupling in nuclear magnetic resonance. *J. Am. Chem. Soc.* **1963**, *85*, 2870–2871.
- (64) Bottaro, S.; Bussi, G.; Pinamonti, G.; Reißer, S.; Boomsma, W.; Lindorff-Larsen, K. Barnaba: software for analysis of nucleic acid structures and trajectories. *RNA* **2019**, *25*, 219–231.
- (65) Condon, D. E.; Kennedy, S. D.; Mort, B. C.; Kierzek, R.; Yildirim, I.; Turner, D. H. Stacking in RNA: NMR of Four Tetramers Benchmark Molecular Dynamics. *J. Chem. Theory Comput.* **2015**, *11*, 2729–2742.
- (66) Zhao, J.; Kennedy, S. D.; Berger, K. D.; Turner, D. H. Nuclear Magnetic Resonance of Single-Stranded RNAs and DNAs of CAAU and UCAAUC as Benchmarks for Molecular Dynamics Simulations. *J. Chem. Theory Comput.* **2020**, *16*, 1968–1984.
- (67) Bottaro, S.; Bussi, G.; Kennedy, S. D.; Turner, D. H.; Lindorff-Larsen, K. Conformational ensembles of RNA oligonucleotides from integrating NMR and molecular simulations. *Science Adv.* **2018**, *4*, eaar8521.

- (68) Gray, P. G.; Kish, L. Survey Sampling. *J. Royal Stat. Soc. A (General)* **1969**, *132*, 272.
- (69) Rangan, R.; Bonomi, M.; Heller, G. T.; Cesari, A.; Bussi, G.; Vendruscolo, M. Determination of structural ensembles of proteins: restraining vs reweighting. *J. Chem. Theory Comput.* **2018**, *14*, 6632–6641.
- (70) Flyvbjerg, H.; Petersen, H. G. Error estimates on averages of correlated data. *J. Chem. Phys.* **1989**, *91*, 461–466.
- (71) Bonomi, M.; Bussi, G.; Camilloni, C.; Tribello, G. A.; Banáš, P.; Barducci, A.; Bernetti, M.; Bolhuis, P. G.; Bottaro, S.; Branduardi, D., et al. Promoting transparency and reproducibility in enhanced molecular simulations. *Nat. Methods* **2019**, *16*, 670–673.
- (72) Chen, A. A.; García, A. E. High-resolution reversible folding of hyperstable RNA tetraloops using molecular dynamics simulations. *Proc. Natl. Acad. Sci. U.S.A.* **2013**, *110*, 16820–16825.
- (73) Kuhrova, P.; Banáš, P.; Best, R. B.; Sponer, J.; Otyepka, M. Computer folding of RNA tetraloops? Are we there yet? *J. Chem. Theory Comput.* **2013**, *9*, 2115–2125.
- (74) Yang, C.; Lim, M.; Kim, E.; Pak, Y. Predicting RNA Structures via a Simple van der Waals Correction to an All-Atom Force Field. *J. Chem. Theory Comput.* **2017**, *13*, 395–399.
- (75) Gil-Ley, A.; Bottaro, S.; Bussi, G. Empirical corrections to the amber RNA force field with target metadynamics. *J. Chem. Theory Comput.* **2016**, *12*, 2790–2798.
- (76) Aytenfisu, A. H.; Spasic, A.; Grossfield, A.; Stern, H. A.; Mathews, D. H. Revised RNA Dihedral Parameters for the Amber Force Field Improve RNA Molecular Dynamics. *J. Chem. Theory Comput.* **2017**, *13*, 900–915.

- (77) Bergonzo, C.; Cheatham III, T. E. Improved force field parameters lead to a better description of RNA structure. *J. Chem. Theory Comput.* **2015**, *11*, 3969–3972.
- (78) Lescoute, A.; Leontis, N. B.; Massire, C.; Westhof, E. Recurrent structural RNA motifs, Isostericity Matrices and sequence alignments. *Nucleic Acids Res.* **2005**, *33*, 2395–2409.
- (79) Bottaro, S.; Gil-Ley, A.; Bussi, G. RNA folding pathways in stop motion. *Nucleic Acids Res.* **2016**, *44*, 5883–5891.
- (80) Zhao, J.; Kennedy, S. D.; Berger, K. D.; Turner, D. H. Nuclear Magnetic Resonance of Single-Stranded RNAs and DNAs of CAAU and UCAAUC as Benchmarks for Molecular Dynamics Simulations. *Journal of Chemical Theory and Computation* **2020**, *16*, 1968–1984.
- (81) Bottaro, S.; Banáš, P.; Šponer, J.; Bussi, G. Correction to “Free Energy Landscape of GAGA and UUCG RNA Tetraloops”. *J. Phys. Chem. Lett.* **2018**, *9*, 1674.
- (82) Kührová, P.; Mlýnský, V.; Zgarbová, M.; Krepl, M.; Bussi, G.; Best, R. B.; Otyepka, M.; Šponer, J.; Banáš, P. Correction to “Improving the performance of the AMBER RNA force field by tuning the hydrogen-bonding interactions”. *J. Chem. Theory Comput.* **2020**, *16*, 818–819.
- (83) Bottaro, S.; Nichols, P. J.; Vögeli, B.; Parrinello, M.; Lindorff-Larsen, K. Integrating NMR and simulations reveals motions in the UUCG tetraloop. *Nucleic Acids Res.* **2020**, *48*, 5839–5848.
- (84) Krepl, M.; Réblová, K.; Koca, J.; Sponer, J. Bioinformatics and Molecular Dynamics Simulation Study of L1 Stalk Non-Canonical rRNA Elements: Kink-Turns, Loops, and Tetraloops. *The journal of physical chemistry. B* **2013**, *117*.
- (85) Goodfellow, I.; Bengio, Y.; Courville, A. *Deep learning*; MIT press, 2016.

- (86) Calonaci, N.; Jones, A.; Cuturello, F.; Sattler, M.; Bussi, G. Machine learning a model for RNA structure prediction. *NAR Genom. Bioinform.* **2020**, *2*, lqaa090.
- (87) Nichols, P. J.; Henen, M. A.; Born, A.; Strotz, D.; Güntert, P.; Vögeli, B. High-resolution small RNA structures from exact nuclear Overhauser enhancement measurements without additional restraints. *Commun. Biol.* **2018**, *1*, 1–11.
- (88) Cate, J. H.; Gooding, A. R.; Podell, E.; Zhou, K.; Golden, B. L.; Kundrot, C. E.; Cech, T. R.; Doudna, J. A. Crystal structure of a group I ribozyme domain: principles of RNA packing. *Science* **1996**, *273*, 1678–1685.
- (89) Batey, R. T.; Rambo, R. P.; Doudna, J. A. Tertiary motifs in RNA structure and folding. *Angew. Chem. Int. Ed.* **1999**, *38*, 2326–2343.
- (90) Tamura, M.; Holbrook, S. R. Sequence and structural conservation in RNA ribose zippers. *J. Mol. Biol.* **2002**, *320*, 455–474.
- (91) Mokdad, A.; Krasovska, M. V.; Sponer, J.; Leontis, N. B. Structural and evolutionary classification of G/U wobble basepairs in the ribosome. *Nucleic Acids Res.* **2006**, *34*, 1326–1341.
- (92) Nissen, P.; Ippolito, J. A.; Ban, N.; Moore, P. B.; Steitz, T. A. RNA tertiary interactions in the large ribosomal subunit: the A-minor motif. *Proc. Natl. Acad. Sci. U.S.A.* **2001**, *98*, 4899–4903.